Evaluation of Multi-Channel ADCs for Gamma-Ray Spectroscopy

Hui Tan, Wolfgang Hennig, Mark D. Walby, Dimitry Breus, and Jackson Harris

***Abstract*—As nuclear physicists increasingly design large scale experiments with hundreds or thousands of detector channels, there are growing needs for high density readout electronics with good timing and energy resolution that at the same time offer lower cost per channel compared to existing commercial solutions. Recent improvements in the design of commercial analog to digital converters (ADCs) have resulted in a variety of multi-channel ADCs that are natural choice for designing such high density readout modules. However, multi-channel ADCs typically are designed for medical imaging/ultrasound applications and therefore are not rated for their spectroscopic characteristics. In this work, we evaluated the gamma-ray spectroscopic performance of several multi-channel ADCs, including their energy resolution, nonlinearity, and timing resolution. Some of these ADCs demonstrated excellent energy resolution, 2.66% FWHM at 662 keV with a $LaBr_3$ or 1.78 keV FWHM at 1332.5 keV with a high purity germanium (HPGe) detector, and sub-nanosecond timing resolution with $LaBr_3$. We present results from these measurements to illustrate their suitability for gamma-ray spectroscopy.**

***Index Terms*—Energy resolution, multi-channel ADC, nonlinearity, timing resolution.**

I. Introduction

MAJOR upgrades and new construction projects at nuclear research facilities are being carried out in the U.S. and abroad to allow nuclear scientists to deliver significant discoveries and advancements in the decades to come. One notable example is the Facility for Rare Isotope Beams (FRIB), which is being designed and constructed at the Michigan State University and will provide intense beams of rare isotopes that allow scientists to better understand the physics of nuclei, nuclear astrophysics, and fundamental interactions [1]. In order to support operations at facilities like FRIB, development of new generations of detectors and readout electronics is critically needed.

As nuclear physics readout electronics increasingly go from analog to digital, digital readout electronics instrumenting radiation detectors have experienced significant advancements in the last decade. This on one hand can be attributed to steady improvements in commercial digital processing components such as analog-to-digital converters (ADCs), digital-to-analog converters (DACs), field-programmable-gate-arrays (FPGAs), and digital-signal-processors (DSPs); on the other hand, this can also be attributed to increasing needs for improved time, position, and energy resolution in nuclear physics experiments, which have spurred the rapid development of commercial off-the-shelf (COTS) high speed, high resolution digitizers or spectrometers. Absent from conventional analog electronics, the capability to record fast decaying pulses from radiation detectors in digital readout electronics has profoundly benefited nuclear physics researchers since they now can perform detailed pulse processing for applications such as gamma-ray tracking and decay-event selection and reconstruction.

Nuclear physicists are increasingly designing large scale radiation detectors to either increase detection efficiency or improve accuracy of position measurement. However, existing COTS readout electronics are prohibitively expensive for large scale radiation detectors. Therefore, there are growing needs for high density, low cost readout electronics. Space saving and low power multi-channel ADCs are then natural choice for designing such high density readout modules. With either 4 or 8 channels integrated on a single chip, these ADCs have a wide range of bits (10 to 16) and sampling rates (40 to 250 MSPS), and generally consume very low power (as low as $\sim$50 mW per channel). Further, ADCs with built-in variable-gain amplifier (VGA) and anti-aliasing filter (AAF) are ideal for applications demanding low power and high level of integration. However, as they are typically designed for medical imaging/ultrasound applications, multi-channel ADCs do not rate for their spectroscopic characteristics in their datasheets. In this work, we present results from our evaluation of several multi-channel ADCs for their gamma-ray spectroscopic performance.

II. Hardware Development

After carefully reviewing datasheet specifications of multi-channel ADCs that are currently available from several ADC vendors, we chose three different types of multi-channel ADCs for our evaluation: AD9222 (Analog Devices), and ADS6425 (Texas Instruments), and AFE5801 (Texas Instruments). Table I lists their datasheet specifications. The AFE5801 ADC has built-in VGA and AAF, and that is probably the reason why no integral nonlinearity (INL) or differential nonlinearity (DNL) is specified in its datasheet. For the purpose of comparing performance of these multi-channel ADCs to that of single channel ADCs that have proven spectroscopic performance, the AD9432 (single channel, 12-bit, 100 MSPS) used on XIA's Pixie-16 spectrometer [2] was also tested. Its datasheet specifications are included in Table I as well. However, no RMS noise number was directly specified in datasheets of AFE5801 and AD9432. The AD9432 and

Manuscript received June 15, 2012; revised November 01, 2012; accepted January 14, 2013. Date of publication March 12, 2013; date of current version April 10, 2013. This work was supported in part by the U.S. Department of Energy under Grant DE-SC0006318.

The authors are with XIA LLC, Hayward, CA 94544 USA (e-mail: htan@xia.com).

Color versions of one or more of the figures in this paper are available online at http://ieeexplore.ieee.org.

Digital Object Identifier 10.1109/TNS.2013.2243468

0018-9499/$31.00 © 2013 IEEE

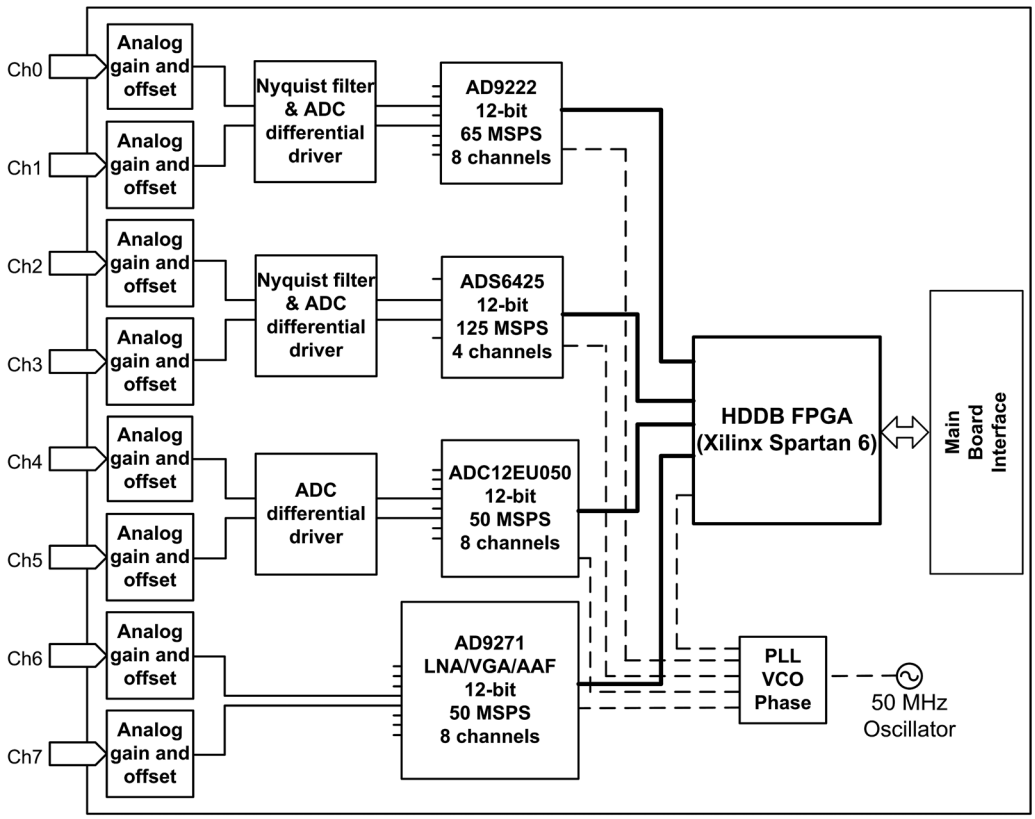

Fig. 1. Block diagram of the prototype board HDDB.

TABLE I
ADC SPECIFICATIONS

Parameter	AD9222	ADS6425	AFE5801	AD9432
Bits	12	12	12	12
Channels	8	4	8	1
Rate (MSPS)	65	125	50	100
Input voltage (Vp-p)	2	2	2	2
VGA	No	No	Yes	No
AAF	No	No	Yes	No
INL (max, LSB)	± 1.0	± 2.5		± 1.0
INL (typ, LSB)	± 0.4	± 1.0		± 0.5
DNL (max, LSB)	± 0.65	+2.0/-0.9		± 0.75
DNL (typ, LSB)	± 0.3	± 0.5		± 0.25
Effective number of bits	11.38	11.4		11.0
Power/channel (mW)	114	325	58	850
Supply voltages (V)	1.8	3.3	1.8, 3.3	3.3, 5
RMS noise (LSB)	0.27	0.407		

AD9222 have about the same INL and DNL while ADS6425 has about twice as much as those of AD9432 based on their respective datasheets. Among the chosen multi-channel ADCs for this study, the AD9222 has been reported as being used in CAEN's V1740 digitizers [3] as well as other front end readout electronics [4], [5], and the AFE5801 is being used in National Instruments' 32-channel digitizer 5752 [6]. However, no detailed gamma-ray spectroscopic performance of these ADCs was reported.

XIA has previously built a multi-channel digital readout module (MicroCAL) for reading out large arrays of microcalorimeter detectors [7]. The MicroCAL module consists of a main board and a daughter board. The main board is a 3U PXI card which accepts digital data stream from a daughter board through inter-board connectors. It also has a 512MB DDR SDRAM that can be used to store a large number of waveforms from the daughter board ADCs before they are read out by the host computer through a PXI/PCI interface. We used the MicroCAL main board as the backend communication and waveform storage board while we designed and built a new daughter board (HDDB) for evaluating two of the three chosen multi-channel ADCs, AD9222 and ADS6425. Fig. 1 shows a block diagram of the HDDB. Only two channels of the AD9222 and ADS6425 have been connected to analog inputs from the front panel connectors due to board space limitation. Further, the other two ADCs on the HDDB, i.e., ADC12EU050 and AD9271, were not evaluated in this study due to project time constraints. Tests on the AFE5801 ADCs were done using another similar XIA in-house test board.

Serial data outputs from these multi-channel ADCs on the HDDB were first deserialized and then processed for pulse detection and waveform capture by an onboard FPGA (Xilinx Spartan-6 LX100T). Captured waveforms, each of which had 16384 samples, were first stored in the HDDB FPGA buffers. The main board FPGA then read those waveforms and wrote to its SDRAM before the host software read these waveforms from the SDRAM and stored them on hard drives. Fig. 2 shows a picture of the combination of the MicroCAL main board and the HDDB.

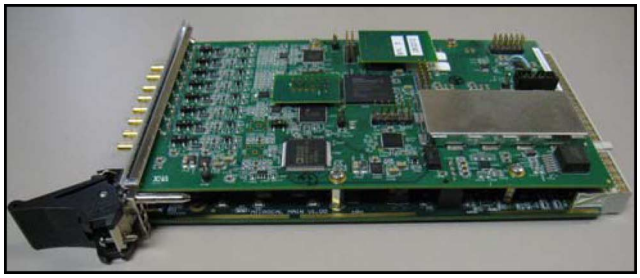

Fig. 2. Picture of high density prototype board HDDB (top) and MicroCAL main board (bottom).

Recorded waveforms from the multi-channel ADCs were processed offline to characterize the timing, energy resolutions and nonlinearity of these ADCs in order to evaluate their suitability for gamma ray spectroscopy.

III. Energy Resolution Measurement

Energy resolution of these ADCs were measured using both high purity germanium (HPGe) and $LaBr_3$ detectors. XIA's pulse height computation algorithm [8] was applied offline to the recorded waveforms to compute energies for all detector pulses contained in the waveforms (one recorded waveform could have more than one detector pulses) except that the AD9432 (Pixie-16) and the AFE5801 obtained their energy spectra from online processing using the same algorithm implemented in the FGPA and DSP. Energy histograms from these ADCs were then calibrated using either multiple peaks from a mix of radioactive sources (HPGe spectra) or the 661.6 keV peak of ^{137}Cs ($LaBr_3$ spectra). The energy resolution (FWHM) of major energy peaks on each spectrum was then computed. Pixie-16's energy resolution represents the state-of-the-art in achievable resolution due to its online processing algorithm and the excellent specifications for its ADC.

A. HPGe

A 40% coaxial HPGe detector was used to measure the energy resolution of the multi-channel ADCs with multiple sources (^{57}Co, ^{22}Na, ^{137}Cs, ^{60}Co, ^{109}Cd, ^{133}Ba, and a ^{232}Th lens). The input count rate was $\sim$3000 cps. Fig. 3 shows the energy spectra from two channels of AD9222, ADS6425, AFE5801 and one channel of Pixie-16, i.e., AD9432, respectively. The number of counts in each spectrum is as follows: AD9222-$\sim 3.2 \times 10^5$; ADS6425-$\sim 2.1 \times 10^5$; AFE5801-$\sim 5.6 \times 10^6$; AD9432-$\sim 6 \times 10^6$. Counts variations resulted primarily from the processing modes, i.e., offline (AD9222 and ADS6425) in which raw waveform data had to be stored on computer disks first or online (AFE5801 and AD9432) in which pulses were processed directly. Nevertheless, counts from both modes were sufficient for quantifying the energy resolution.

As shown in Table II, excellent HPGe energy resolution was achieved by the 8-channel 65 MSPS AD9222. In fact, its energy resolution was very close to that of the state-of-the-art Pixie-16 ADC, i.e., the single channel, 12-bit, 100 MSPS AD9432. The energy resolution of the 4 channel 125 MSPS ADS6425 was slightly worse than that of the AD9222. This was not surprising given the slightly worse datasheet specifications

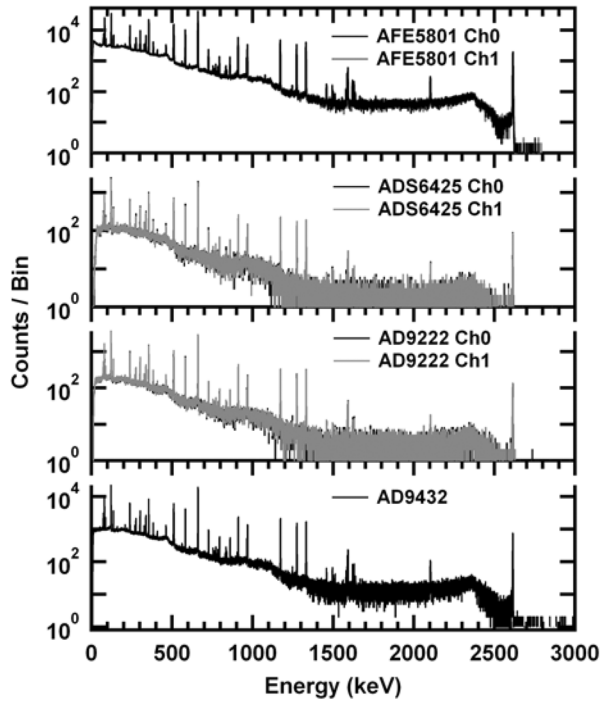

Fig. 3. Energy spectra from a 40% coaxial HPGe detector and multiple radiation sources.

TABLE II
HPGe Energy Resolution (keV, FWHM)

Energy (keV)	AD9222		ADS6425		AFE5801		AD9432
	Ch0	Ch1	Ch0	Ch1	Ch0	Ch1	
122	0.92	0.92	0.98	1.08	1.15	1.16	0.84
661.6	1.34	1.36	1.36	1.43	1.55	1.55	1.28
1332.5	1.78	1.80	1.84	1.82	1.96	1.96	1.72
2614.5	2.39	2.44	2.47	2.52	2.64	2.63	2.36

for the ADS6425 in terms of nonlinearity and RMS noise. Compared to the other three ADCs, the AFE5801 had slightly worse energy resolution even though such resolution was still sufficiently good for general purpose gamma-ray spectroscopy.

Another observation that can be made about these multi-channel ADCs is that there is little variation in energy resolution between two channels of the same ADC. That demonstrated not only the uniformity of these ADCs but also their minimal crosstalk between channels.

B. $LaBr_3$

A $1'' \times 1''$ cylindrical $LaBr_3$ crystal coupled to a $2''$ PMT (Photonis XP2020) radiated with ^{137}Cs was also used to measure the energy resolution of these ADCs. Fig. 4 shows the energy spectra from two channels of AD9222, ADS6425, AFE5801 and one channel of Pixie-16, respectively. Both AD9222 and ADS6425 achieved excellent energy resolution: 2.66% FWHM for ADS6425 or an average of 2.84% for two channels of AD9222, compared to 3.05% for the Pixie-16 ADC AD9432.

Even at its lowest gain setting, the Pixie-16 still had the highest gain set for its ADC among all four tested ADCs. In order to ensure $LaBr_3$/PMT pulses coming into the Pixie-16

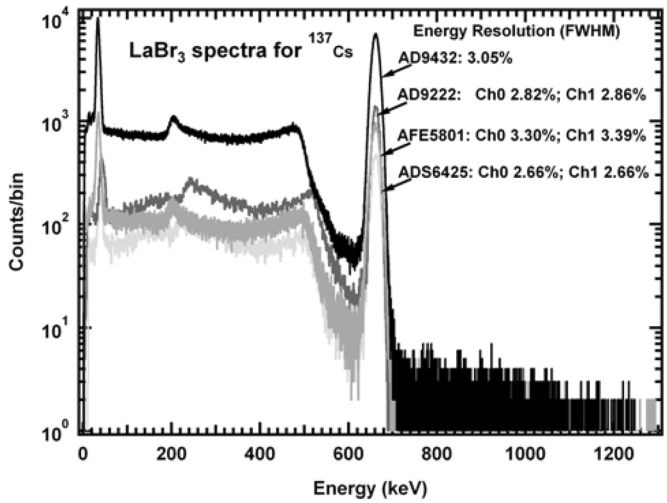

Fig. 4. Energy spectra from a $1'' \times 1''$ cylindrical $LaBr_3$ crystal coupled to a $2''$ PMT irradiated with ^{137}Cs.

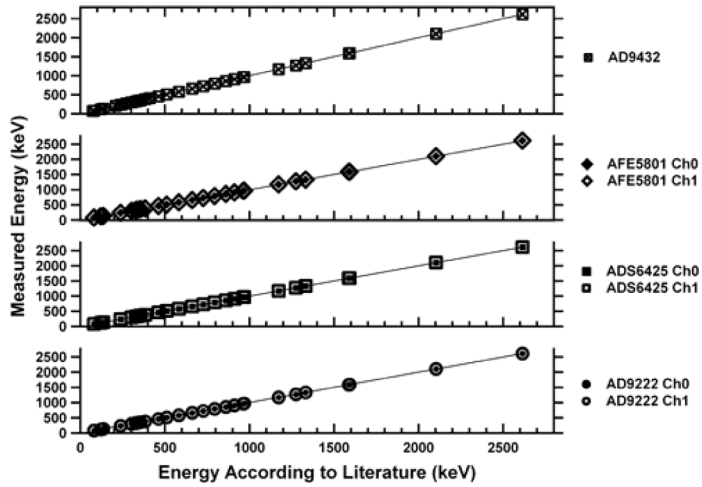

Fig. 5. Measured energy versus nominal energy for the ADCs.

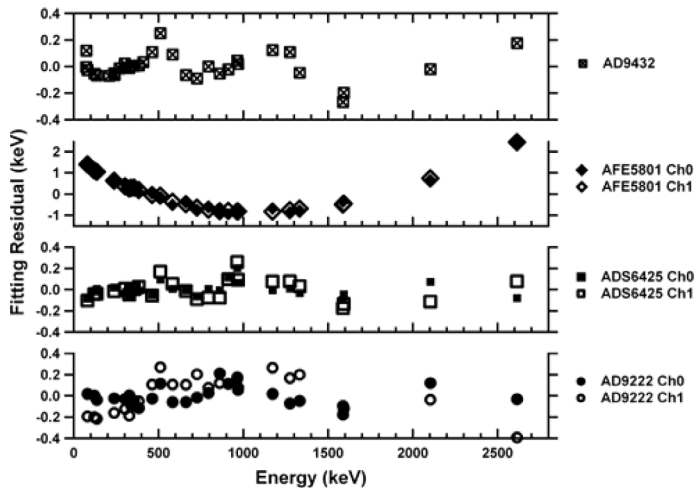

Fig. 6. Residuals from linear fit.

were within its ADC voltage range, we had to attenuate them with multiple 50 Ω terminators. We suspected that might have contributed to the slightly worse $LaBr_3$ energy resolution for AD9432. The AFE5801's resolution was also slightly worse at $\sim$3.3%. Difference in the location of the Compton edge was observed between the AD9432 & AFE5801 spectra and the AD9222 & ADS6425 spectra, but that was caused by the location of ^{137}Cs (inside the PMT box in one case and outside the box in the other) and should not affect the energy resolution measurement.

IV. Nonlinearity Measurement

Measurements of multi-channel ADCs' nonlinearity were performed using the same 40% coaxial HPGe detector with reference radiation sources as a source of pulses with defined height. This test characterizes the effect of integral nonlinearity in the spectrometer operation. The measurement was done as follows.

Using the same HPGe energy spectra that were used to characterize the energy resolution of each ADC, the four peaks corresponding to the four energies in Table II were first identified in each spectrum. Gaussian fits were subsequently performed on each peak and the four peak positions in raw spectrum bin units were used to linearly scale the entire spectrum to keV units. Finally a peak finding routine was applied to the newly scaled spectrum to find the energy peaks that were associated with known energies of radiation sources used during the data acquisition. Plotting the measured energies versus nominal energies gives plots shown in Fig. 5. Linear fits were then performed on every set of measured energies versus nominal energies, and their residual from the linear fit was plotted and shown in Fig. 6.

Table III summarizes the linear fit residuals of the four ADCs. In terms of RMS of the deviations, both ADS6425 and AD9432 were at or below 0.1 keV. While channel 0 of AD9222 showed excellent RMS of deviations at 0.09 keV, its channel 1 had slightly elevated residuals, as did the range of deviations between maximum and minimum values. The AFE5801 had

TABLE III
Integral Nonlinearity as Represented by Residual From Linear Fit of HPGe Measured Energies Versus Nominal Energies (keV)

Nonlinearity	AD9222		ADS6425		AFE5801		AD9432
	Ch0	Ch1	Ch0	Ch1	Ch0	Ch1	
RMS of deviations	0.09	0.17	0.07	0.10	0.83	0.83	0.10
Maximum deviation	+0.21	+0.27	+0.20	+0.26	+2.45	+2.45	+0.25
Minimum deviation	-0.18	-0.39	-0.09	-0.18	-0.91	-0.83	-0.27

the worst integral nonlinearity among the four ADCs, and that might be attributable to its built-in VGA. However, it would be relatively easy to correct the integral nonlinearity of the AFE5801 even in online processing mode due to its relatively easy-to-define "bowl" like shape of its residuals versus energy curve.

One way to characterize the DNL of an ADC is the histogram test method. It involves collecting a large number of digitized samples from a well-defined input signal with a known probability density function. A slow linear ramp (relative to the ADC sampling time intervals), which slightly exceeds both ends of

TABLE IV
DIFFERENTIAL NONLINEARITY MEASURED USING THE HISTOGRAM TEST METHOD (12-BIT ADC LSB)

Nonlinearity	AD9222		ADS6425		AFE5801		AD9432
	Ch0	Ch1	Ch0	Ch1	Ch0	Ch1	
RMS of deviations	0.10	0.11	0.18	0.16	0.02	0.02	0.08
Maximum deviation	+0.37	+0.36	+0.64	+0.59	0.11	0.09	+0.30
Minimum deviation	-0.33	-0.30	-0.53	-0.50	-0.11	-0.11	-0.48

the range of the ADC, is a good choice as the input signal to the ADC. The number of occurrences of each ADC code bin is tallied from the collected samples. If the ADC has no DNL errors, all codes should have equal probability of occurrence (with the exception of the ADC end-point all "0"s and all "1"s codes). Deviations from the equal probability are quantified as the DNL errors of the ADC. For this measurement, we used a high precision waveform generator (Agilent 33522A) to generate linear ramps with frequency of 10 Hz, amplitude of 2 Vpp, and 100% symmetry. Fig. 6 shows the measured ADC DNL using this histogram test method, and Table IV summarizes the DNL distributions of each ADC.

When comparing the measured DNL values to the datasheet specifications of three of the four tested ADCs (AFE5801's datasheet does not specify its DNL or INL), they matched quite well to the datasheet values. For instance, the measured maximum and minimum DNL of the AD9222 is $+0.37$ LSB and -0.33 LSB, respectively, whereas its datasheet quotes typical DNL at ± 0.3 LSB and maximum DNL at ± 0.65 LSB. In the case of the AD9432, the datasheet specifies typical DNL at ± 0.25 LSB and maximum DNL at ± 0.75 LSB. The measured DNL is certainly within such specifications. The measured AFE5801 DNL is relatively low compared to the other ADCs. However, there is a distinctive "bowl" like shape for the AFE5801 DNL curve, and the errors are tilted more towards negatives than positives.

V. TIMING RESOLUTION MEASUREMENT

We measured the timing precision of these ADCs using two same sets of $LaBr_3$ crystal and PMT that were used in the energy resolution measurement. Two channels of each ADC (in the case of AD9432 two ADCs were used) first captured simultaneously waveforms from $LaBr_3$/PMT detectors irradiated by either ^{137}Cs or ^{22}Na. Time jitters between these two channels were then measured by analyzing the waveforms offline using an algorithm that computed the time difference between their rising edges. For each edge, the algorithm determined the point where the pulse crossed a constant fraction threshold by linear interpolation of the two closest samples to sub-sample precision.

Fig. 8 shows sample ^{137} Cs traces captured by those four different ADCs from the same $LaBr_3$/PMT detector. Their baseline levels were different at the output of their respective ADCs, but were adjusted to be same offline for display purpose. Since they all corresponded to the same 661.6 keV gamma-rays, their amplitude differences reflected the different gains as well as the external signal attenuations that were applied to the input signals

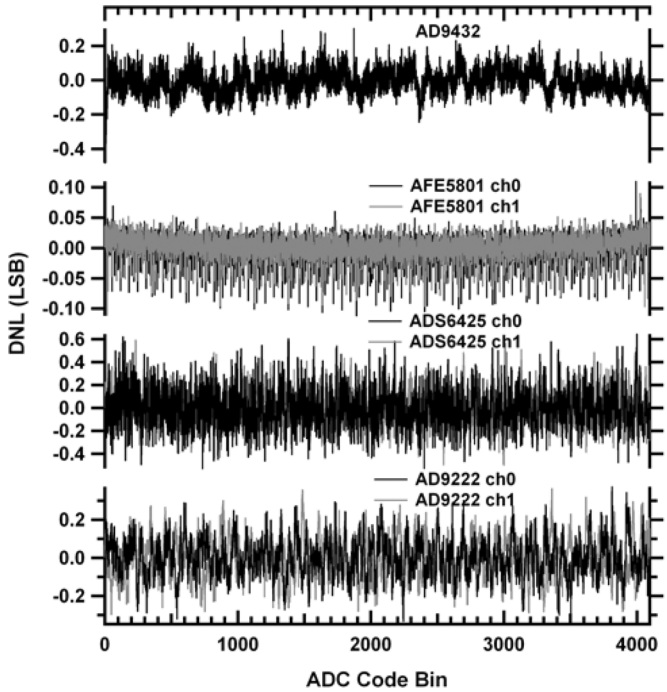

Fig. 7. Measured ADC DNL using the histogram test method.

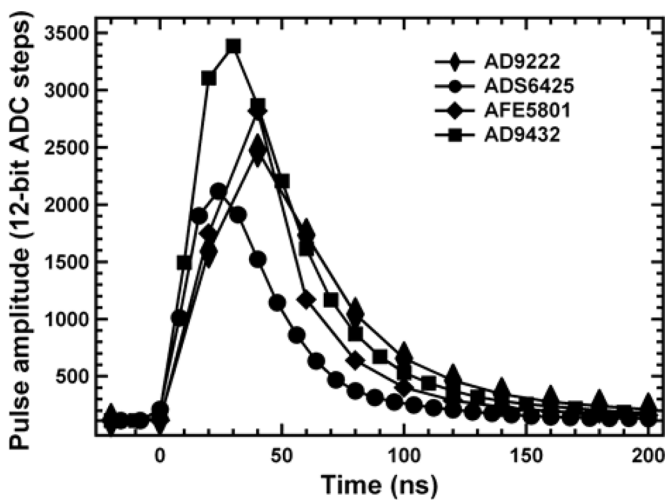

Fig. 8. Sample 661.6 keV ^{137}Cs traces captured by the ADCs from a $1'' \times 1''$ cylindrical $LaBr_3$ crystal coupled to a $2''$ PMT.

to these ADCs. What was interesting to notice on these ADC traces was the number of points on their respective rising edge. Due to the different sampling rates of these ADCs, there were 4 data points on the rising edge of the pulses from AD9432 (100 MSPS) and ADS6425 (125 MSPS), but only 2 data points for AD9222 (65 MSPS) and AFE5801 (50 MSPS).

A. Single $LaBr_3$/PMT Output Split Into Two Branches

The first method that we used to measure the timing precision of the ADCs is illustrated in Fig. 9. The output of a single $LaBr_3$/PMT detector, irradiated by a ^{137}Cs source, was split into two branches, which were then fed into two channels of the same ADC, or in the case of Pixie-16, two different ADCs. The two branches had about the same cable length. The input signal to

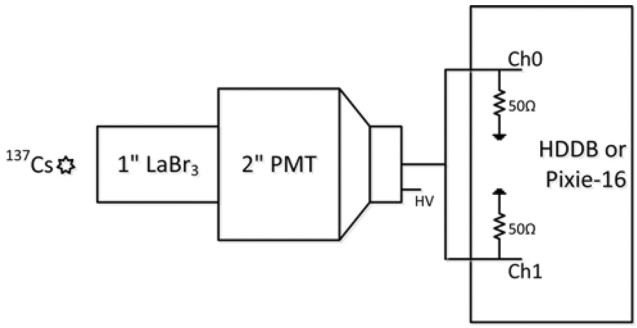

Fig. 9. Experimental setup for measuring timing resolution using a single $LaBr_3$/PMT detector and a ^{137}Cs source. The output of the $LaBr_3$/PMT was split into two branches and then fed into two ADC channels.

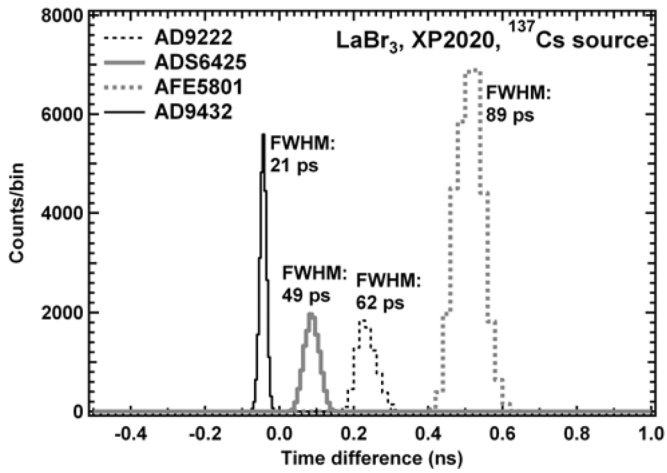

Fig. 10. Histograms of measured time difference between rising edges of $LaBr_3$/PMT pulses using the experimental setup shown in Fig. 8.

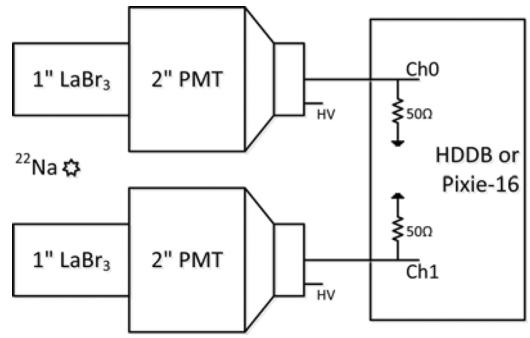

Fig. 11. Experimental setup for measuring timing resolution when using two $LaBr_3$/PMT detectors in coincidence mode with a ^{22}Na source. The two outputs of the two $LaBr_3$/PMT detectors were fed into two ADC channels, respectively.

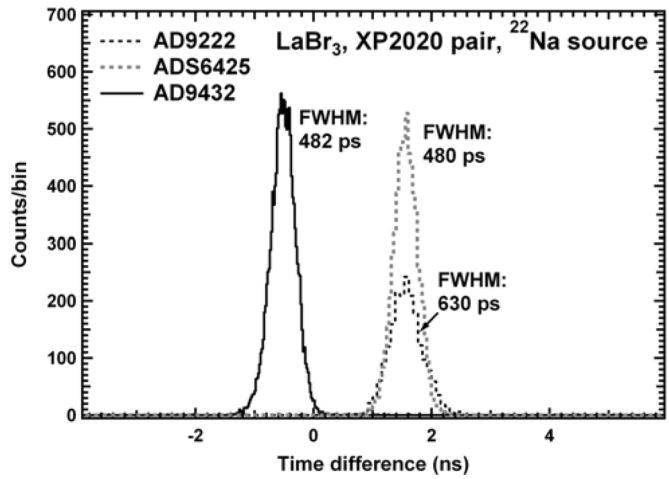

Fig. 12. Histograms of measured time difference between rising edges of $LaBr_3$/PMT pulses using the experimental setup shown in Fig. 10.

the ADCs was terminated with 50 Ω resistors either internally or externally.

Since identical signals were fed into the two ADC channels, this method essentially measured the noise additions to the input signal from each ADC channel's analog signal condition circuits as well as the ADC itself. Fig. 10 shows the four histograms of measured time difference for the four types of ADCs that were tested. Only those waveforms that corresponded to the 661.6 keV photopeak from the ^{137}Cs were used for computing the time difference and histogramming. All four ADCs showed excellent time precision in this experimental setup with time difference FWHM all below 100 ps. The AD9432 used on the Pixie-16 showed the best FWHM of 21 ps among the four. The ADS6425, AD9222 and AFE5801 achieved FWHM 49 ps, 62 ps, and 89 ps, respectively. In comparison, the single channel 12-bit, 500 MSPS ADC ADS5463 reported in [9] achieved 23 ps FWHM using a similar experimental setup.

B. Two $LaBr_3$/PMT Pairs in Coincidence

Fig. 11 shows the second method that was used to measure the timing precision of these ADCs. Coincident signals from two $LaBr_3$/PMT detectors, both irradiated by the same ^{22}Na source, were fed into two channels of the same ADC; or in the case of Pixie-16, two different ADCs. The two branches had about the same cable length. The input signal to the ADCs was again terminated with 50 Ω resistors either internally or externally. Coincidence between the two ADC channels was required before waveforms from these two ADC channels were acquired and stored to disk. Due to project time constraints, FPGA firmware was not programmed to perform coincidence detection for AFE5801. Therefore no coincidence data were acquired for AFE5801 from two $LaBr_3$/PMT detectors.

Fig. 12 shows the three histograms of measured time difference for the three types of ADCs. Only those waveforms that corresponded to the 511 keV photopeak from the ^{22}Na were used for computing the time difference and histogramming. Gaussian fits to these histograms resulted in the following timing values: the 125 MSPS quad channel ADS6425 showed a FWHM of 480 ps whereas the FWHM for the 100 MSPS single channel AD9432 used in the Pixie-16 was 482 ps. The FWHM for the 8-channel 65 MSPS AD9222 was slightly worse at 630 ps. The timing resolution attributed to each channel is then 1/sqrt(2) of these values, i.e., 339 ps, 340 ps, and 445 ps for the ADS6425, AD9432 and AD9222, respectively. In comparison, with a similar experimental setup the single channel 12-bit, 500 MSPS ADC ADS5463 achieved $\sim$250 ps FWHM [9].

VI. Conclusion

Multi-channel ADCs AD9222 and ADS6425 demonstrated excellent energy resolution with a 40% coaxial HPGe detector, about 1.8 keV FWHM at 1332.5 keV, nearly identical to that of single channel Pixie-16 ADC AD9432. The AFE5801 achieved 1.96 keV FWHM at 1332.5 keV with the HPGe. These multi-channel ADCs showed excellent differential linearity, and by comparison, ADS6425 had the best integral linearity while AFE5801 had the worst integral linearity. Excellent timing resolution was measured with all four ADCs that were tested with $LaBr_3$/PMT detectors: <100 ps in single-detector mode and <1 ns in two-detector coincidence mode (the AFE5801 was not tested in this mode). These results readily demonstrate that these multi-channel ADCs are well suited for gamma-ray spectroscopy.

References

[1] R. York *et al.*, "Status and plans for the facility for rare isotope beams at michigan state university," in *Proc. XXV Linear Accelerator Conf. (LINAC10)*, Tsukuba, Japan, Sep. 12–17, 2010.

[2] K. Starosta *et al.*, "Digital data acquisition system for experiments with segmented detectors at national superconducting cyclotron laboratory," *Nucl. Instr. Meth. A*, vol. 610, pp. 700–709, Nov. 2009.

[3] CAEN V1740, 64 Channel 12 bit 62.5 MS/s Digitizer. [Online]. Available: http://www.caen.it/csite/CaenProd.jsp?parent=11\&idmod=591

[4] M. Bogdan, H. Huan, and S. Wakley, "64-channel, 5 GSPS ADC module with switched capacitor arrays," *Nucl. Instr. Meth. A* [Online]. Available: http://dx.doi.org/10.1016/j.nima.2012.08.087 In Press

[5] H. Chen, G. D. Geronimo, F. Lanni, D. Lissauer, D. Makowiecki, V. Radeka, S. Rescia, C. Thorn, and B. Yu, "Front end readout electronics of the MicroBooNE experiment," *Phys. Procedia*, vol. 37, pp. 1287–1294, 2012.

[6] NI 5752, 32-Channel Digitizer Adapter Module for NDT Applications. [Online]. Available: http://sine.ni.com/nips/cds/view/p/lang/en/nid/208656

[7] H. Tan, J. W. Collins, M. Walby, W. Hennig, W. K. Warburton, and P. Grudberg, "A versatile multichannel digital signal processing module for microcalorimeter arrays," *J. Low Temp. Phys.*, vol. 167, pp. 609–619, June 2012.

[8] H. Tan, M. Momayezi, A. Fallu-Labruyere, Y. X. Chu, and W. K. Warburton, "A fast digital filter algorithm for gamma-ray spectroscopy with double-exponential decaying scintillators," *IEEE Trans. Nucl. Sci.*, vol. 51, no. 4, pp. 1541–1545, Aug. 2004.

[9] W. Hennig, S. J. Asztalos, D. Breus, K. Sabourov, and W. K. Warburton, "Development of 500 MHz multi-channel readout electronics for fast radiation detectors," *IEEE Trans. Nucl. Sci.*, vol. 57, no. 4, pp. 2365–2370, Aug. 2010.